Fermi acceleration and scaling properties of a time dependent oval billiard

Edson D. Leonel,[1] Diego F. M. Oliveira,[2] and Alexander Loskutov[1,3]
[1]*Departamento de Estatística, Matemática Aplicada e Computação, Universidade Estadual Paulista, Av. 24A, 1515 Bela Vista, Rio Claro, São Paulo 13506-900, Brazil*
[2]*Departamento de Física, Universidade Estadual Paulista, Av. 24A, 1515 Bela Vista, Rio Claro, São Paulo 13506-900, Brazil*
[3]*Physics Faculty, Moscow State University, 119899 Moscow, Russia*

(Received 1 April 2009; accepted 24 August 2009; published online 23 September 2009)

We consider the phenomenon of Fermi acceleration for a classical particle inside an area with a closed boundary of oval shape. The boundary is considered to be periodically time varying and collisions of the particle with the boundary are assumed to be elastic. It is shown that the breathing geometry causes the particle to experience Fermi acceleration with a growing exponent rather smaller as compared to the no breathing case. Some dynamical properties of the particle's velocity are discussed in the framework of scaling analysis. © *2009 American Institute of Physics*.
[DOI: 10.1063/1.3227740]

The behavior of the average velocity for the time varying oval-shaped billiard with the breathing geometry is considered. A four dimensional mapping that describes the dynamics of the model is carefully constructed. We show that the average velocity of the particle is described by a scaling function with critical exponents. The exponents obtained do not match the exponents found for the bouncer model (the simplest one-dimensional model exhibiting unlimited energy growth), thus putting the oval billiard in a different class of universality of the bouncer model.

I. INTRODUCTION

Unlimited energy growth for a classical particle suffering elastic collisions with a massive and time varying wall is a phenomenon known as the Fermi acceleration. The phenomenon was first proposed by Fermi[1] in 1949 for studies concerning time moving magnetic fields that accelerate cosmic particles. After that many approaches regarding the description of such a phenomenon were introduced for both the continuous and discrete time modeling. For continuous time evolution, basically differential equations should be solved while the discrete time modeling is made essentially by using the billiard approach. A billiard is defined by a connected region $Q \subset \Re^D$ with the boundary $\partial Q \subset \Re^{D-1}$ separating Q from its complement. A pointlike particle moves freely inside the billiard along geodesic lines until it hits the boundary. For a static boundary, after the collision, it is assumed that the particle reflects specularly (the angle of incidence is equal to the angle of reflection) with an instantaneously change in the momentum component orthogonal to the boundary. For the case of $D=1$ (one-dimensional case) there are many results concerning the description of Fermi acceleration and the three basic models are (i) Fermi–Ulam model,[2–5] (ii) the bouncer model,[6–10] and (iii) the hybrid Fermi–Ulam-bouncer model.[11–13] Case (i) consists of a classical particle of mass m, which is confined to bounce between two walls where one of them is fixed and the other one is periodically moving. It is known that for a sinusoidal motion in time of the moving wall, unlimited energy growth is not expected to be observed. The main reason for such behavior is that the phase space exhibits a mixed form including large chaotic seas surrounding a set of Kolmogorov–Arnold–Moser (KAM) islands and invariant spanning curves limiting the size of chaotic seas. The presence of the invariant spanning curves prevents the particle to experience the unlimited energy growth. However for case (ii), i.e., the bouncer model, which consists of a classical particle falling in a constant gravitational field and suffering elastic collisions with a flat and moving plate, depending on the initial conditions as well as on the control parameters, the particle can experience the unlimited energy growth. Finally, case (iii) consists of a hybrid version of both the Fermi–Ulam and bouncer model. The particle is confined to bounce between two walls; one of them is moving in time (say, the lower) while the other one is assumed to be fixed (the upper). Additionally the particle suffers the action of a constant gravitational field. The phase space of the model has a set of invariant spanning curves at high energy and, depending on the initial conditions and control parameters, properties that were observed individually for both the Fermi–Ulam model and the bouncer model, can come together and coalesce in the hybrid version of the model.

The case of $D=2$ is rather complicate and one of the main questions that should be addressed is the following: Can a classical particle, experiencing deterministic dynamics inside a billiard with periodically moving boundary, be accelerated unlimitedly? The answer for this question is not so simple and basically it depends on the phase portrait of the static version of the model. In this connection, a conjecture proposed in the paper[14] [Loskutov, Ryabov, and Akinshin (LRA) conjecture] says that the Fermi acceleration in time dependent billiards should be observed if they possess chaotic component in the static case. Results that corroborate/motivate to the validity of this conjecture include the time varying circular billiard,[15] the concentric case of the annular

billiard,[16] and the elliptic case.[17] A specific time perturbation in an elliptic billiard model was recently introduced by Lenz *et al.*[18] It therefore leads the system to exhibit a tunable Fermi acceleration. The mechanism that accelerates the particle to unlimited energy is repeated crossings of the separatrix region by the particle's trajectory. It was discussed by Gelfreich and Turaev,[19] a procedure at which a classical particle might acquire unlimited energy growth by using theory of Hamiltonian dynamics. It was also recently shown for a time dependent oval billiard[20] that, in certain cases under the breathing perturbation, the particle does not exhibit unlimited energy growth. As we shall show in the present paper, the breathing geometry can indeed lead the particle to experience Fermi acceleration. However, the slope of growth is rather smaller as compared to the nonbreathing case. The small growing exponent for the average velocity was the main reason that led the authors of Ref. 20, including one of the authors of this paper, to conclude that Fermi acceleration was not observed in the breathing case.

In this paper we revisit the problem of a classical particle bouncing elastically inside a periodically time varying oval billiard. Our main goal is therefore to understand and describe the behavior of the particle's average velocity (and hence its energy) as a function of the number of collisions with the boundary. The problem is described using a four dimensional mapping for the variables: velocity of the particle, the time immediately after a collision with the moving boundary, the angle that the trajectory of the particle does with the tangent at the position of the hit, and the angular position of the particle along the boundary.

The paper is organized as follows. In Sec. II, we present all the details needed to construct the mapping that describes the dynamics of the model. We explore some of the numerical properties of the model in Sec. III. Finally, in Sec. IV we summarize our results and present our concluding remarks.

II. THE MODEL AND THE MAPPING

The model under consideration consists of a classical point particle of mass m, which is suffering elastic collisions with a periodically moving boundary. The shape of the boundary in polar coordinates is given by the expression

$$R_b(\theta,p,\epsilon,\eta_1,\eta_2,t) = 1 + \eta_1 \cos t + \epsilon[1 + \eta_2 \cos t]\cos(p\theta). \tag{1}$$

The parameter ϵ controls the circle deformation, thus recovering the circle shape for $\epsilon=0$. We shall consider only $\epsilon \in [0,1)$ to avoid the boundary to experience self-intersections. The control parameter η_1 defines the circle's time perturbation when η_2 characterizes the oval's time perturbation. The trivial case of $\eta_1=\eta_2=0$ recovers the static oval billiard. The condition where $\eta_1=\eta_2$ defines what was called in a previous paper[20] as the *breathing case*. This kind of boundary defines a generalization in two dimensions for the Fermi–Ulam accelerator model. The dynamics of the model is described in terms of a four dimensional map $T(\theta_n,\alpha_n,V_n,t_n)=(\theta_{n+1},\alpha_{n+1},V_{n+1},t_{n+1})$, where the variables denote, respectively, the angular position of the particle, the angle that the trajectory of the particle does with the tangent line at the position of the collision, the absolute velocity of the particle, and the instant of the hit with the boundary. Figure 1 illustrates the geometry of six successive bounces of the particle with the boundary. Each dotted line corresponds to a snapshot of the boundary at the instant of the collision. The corresponding angles that describe the dynamics are also illustrated in the figure. The case of boundary time independence is shortly illustrated in the Appendix.

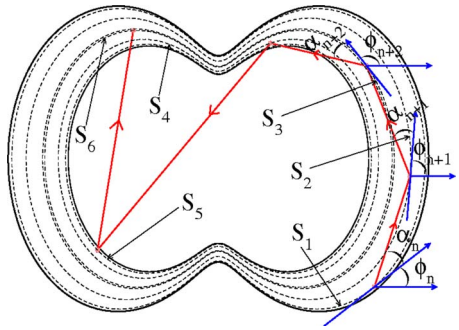

FIG. 1. (Color online) Illustration of six snapshots of a time varying oval billiard. The corresponding angles that describe the dynamics are also illustrated for three collisions.

Given an initial condition $(\theta_n,\alpha_n,V_n,t_n)$ we have all the needed ingredients to construct the mapping T. The two initial coordinates that describe the position of the particle are $X(\theta_n)=R(\theta_n,t_n)\cos(\theta_n)$ and $Y(\theta_n)=R(\theta_n,t_n)\sin(\theta_n)$. The vector velocity of the particle is written as

$$\vec{V}_n = |\vec{V}_n|[\cos(\phi_n+\alpha_n)\hat{i} + \sin(\phi_n+\alpha_n)\hat{j}], \tag{2}$$

where $\hat{i}$ and $\hat{j}$ represent both the unit vectors with respect to the X and Y axis, respectively. The auxiliary angle ϕ_n is defined as

$$\phi_n = \text{atan}\left[\frac{Y'(\theta_n,t_n)}{X'(\theta_n,t_n)}\right], \tag{3}$$

where $X'(\theta_n,t_n)=dX(\theta_n,t_n)/d\theta_n$ and $Y'(\theta_n,t_n)=dY(\theta_n,t_n)/d\theta_n$.

The above expressions allow us to obtain the position of the particle as a function of time for $t \geq t_n$,

$$X_\rho(t) = X(\theta_n) + |\vec{V}_n|\cos(\phi_n+\alpha_n)(t-t_n), \tag{4}$$

$$Y_\rho(t) = Y(\theta_n) + |\vec{V}_n|\sin(\phi_n+\alpha_n)(t-t_n). \tag{5}$$

The index ρ denotes that such coordinates correspond to the particle while the index b [see Eq. (1)] denotes the boundary. The distance of the particle measured with respect to the origin of the coordinate system is given by $R_\rho(t)=\sqrt{X_\rho^2(t)+Y_\rho^2(t)}$. Therefore, the angular position at the next collision of the particle with the boundary, i.e., θ_{n+1}, is obtained by solving the following equation:

$$R_\rho(\theta_{n+1},t_{n+1}) = R_b(\theta_{n+1},t_{n+1}). \tag{6}$$

Moreover, we can also obtain the time at the next collision by just evaluating the expression

$$t_{n+1} = t_n + \frac{\sqrt{[\Delta X_\rho]^2 + [\Delta Y_\rho]^2}}{|V_n|}, \tag{7}$$

where $\Delta X_\rho = X_\rho(\theta_{n+1}) - X_\rho(\theta_n)$ and $\Delta Y_\rho = Y_\rho(\theta_{n+1}) - Y_\rho(\theta_n)$. The next step is then to obtain the new particle's velocity V_{n+1} and the new angle α_{n+1}. To obtain the new velocity, however, we should note that the referential frame of the boundary is moving. Then at the instant of the collision, the following conditions must be matched:

$$\vec{V}'_{n+1} \cdot \vec{T}_{n+1} = \vec{V}'_n \cdot \vec{T}_{n+1}, \tag{8}$$

$$\vec{V}'_{n+1} \cdot \vec{N}_{n+1} = -\vec{V}'_n \cdot \vec{N}_{n+1}, \tag{9}$$

where the upper prime indicates that the velocity of the particle is measured with respect to the moving wall referential frame. At the new angular position θ_{n+1} both the unitary tangent and normal vectors are

$$\vec{T}_{n+1} = \cos(\phi_{n+1})\hat{i} + \sin(\phi_{n+1})\hat{j}, \tag{10}$$

$$\vec{N}_{n+1} = -\sin(\phi_{n+1})\hat{i} + \cos(\phi_{n+1})\hat{j}, \tag{11}$$

so that we can easily find that

$$\vec{V}_{n+1} \cdot \vec{T}_{n+1} = |\vec{V}_n|[\cos(\alpha_n + \phi_n)\cos(\phi_{n+1})] + |\vec{V}_n|[\sin(\alpha_n + \phi_n)\sin(\phi_{n+1})], \tag{12}$$

$$\vec{V}_{n+1} \cdot \vec{N}_{n+1} = -|\vec{V}_n|[-\cos(\alpha_n + \phi_n)\sin(\phi_{n+1})] - |\vec{V}_n|[\sin(\phi_n + \alpha_n)\cos(\phi_{n+1})] + 2\vec{V}_b(t_{n+1}) \cdot \vec{N}_{n+1}, \tag{13}$$

where $\vec{V}_b$ is the velocity of the boundary, which is written as

$$\vec{V}_b(t_{n+1}) = \frac{dR_b(t_{n+1})}{dt_{n+1}}[\cos(\theta_{n+1})\hat{i} + \sin(\theta_{n+1})\hat{j}], \tag{14}$$

where

$$\frac{dR_b(t_{n+1})}{dt_{n+1}} = -\eta_1 \cos(t_{n+1}) - \eta_2 \epsilon \sin(t_{n+1})\cos(p\theta_{n+1}). \tag{15}$$

Then we have that $V_{n+1} = \sqrt{(\vec{V}_{n+1} \cdot \vec{T}_{n+1})^2 + (\vec{V}_{n+1} \cdot \vec{N}_{n+1})^2}$. Finally the angle α_{n+1} is written as

$$\alpha_{n+1} = \text{atan}\left[\frac{\vec{V}_{n+1} \cdot \vec{N}_{n+1}}{\vec{V}_{n+1} \cdot \vec{T}_{n+1}}\right]. \tag{16}$$

It is shown in Fig. 2 the behavior of the average velocity of the particle, for a single orbit, as a function of the number of collisions with the boundary. The control parameters used were $p=2$, $\epsilon=0.4$ and two different initial velocities $V_0=5$ and $V_0=10$. The parameters η_1 and η_2 are labeled in the figure. The procedure used to obtain the solution of Eq. (6) is basically the molecular dynamics. The numerical simulations shown in Fig. 2 have been performed in FORTRAN using quadruple precision with an accuracy of 10^{-26}. Additionally, we have evolved our simulations up to 10^9 collisions with the boundary. The average velocity shown in Fig. 2 was obtained

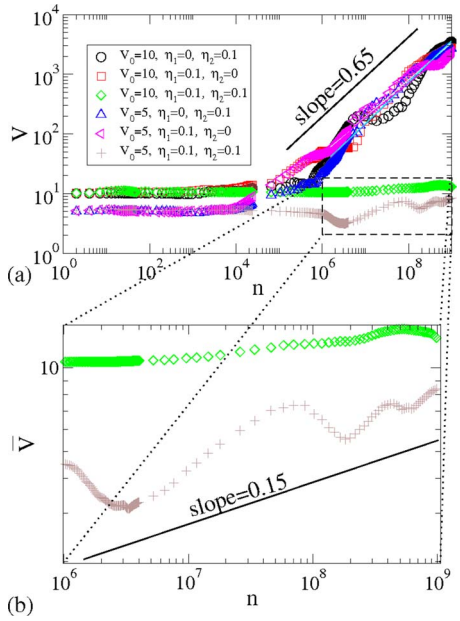

FIG. 2. (Color online) Behavior of $\bar{V}$ vs n. The control parameters used in the construction of the figure were $p=2$, $\epsilon=0.4$ and two different initial velocities $V_0=5$ and $V_0=10$. The parameters η_1 and η_2 are labeled in the figure.

by evaluating $\bar{V}=1/n\Sigma_{k=1}^{n} V_k$, which is basically the average over the orbit. The characterization of the average velocity for the oval-shaped billiards furnishes critical exponents that could be compared to those obtained for the one-dimensional bouncer model (a particle bouncing elastically a moving wall in the presence of a gravitational field). The bouncer model is the simplest one-dimensional model exhibiting Fermi acceleration.

We can clearly see that the nonbreathing geometry leads to a very fast average velocity growth with an average exponent of the order of 0.65. However, and contrary to what a short simulation shows, the breathing case [see Fig. 2(b)] does indeed lead to a lower average velocity increase. The average exponent, obtained for a single orbit (that one shown in cross), gives that the slope of growth is of the order of 0.15. The convincing confirmation of Fermi acceleration is shown in Fig. 3 for very long simulations of 10^9 collisions of the particle with the boundary for the control parameters

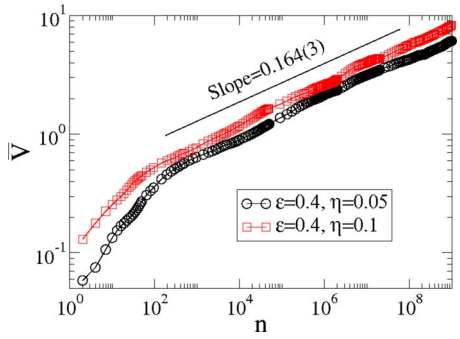

FIG. 3. (Color online) Behavior of $\bar{V}$ vs n. The control parameters used in the construction of the figure were $p=2$, $\epsilon=0.4$ and two different values for η, namely, $\eta=0.1$ and $\eta=0.05$. The slope of growth is 0.164(3).

$p=2$, $\epsilon=0.4$ and two values of η, namely, $\eta=\eta_1=\eta_2=0.1$ and $\eta=\eta_1=\eta_2=0.05$. We see that the average velocity $\bar{V}$ reaches almost the value of 10. Moreover, the average velocity is still growing from there, therefore, confirming Fermi acceleration for the breathing case.

From now on, we shall consider only the breathing case, i.e., the situation where $\eta_1=\eta_2=\eta$. Thus, the radius of the boundary in polar coordinates is written as

$$R_b(\theta,p,\epsilon,\eta,t)=[1+\eta\cos t][1+\epsilon\cos(p\theta)]. \tag{17}$$

III. SCALING PROPERTIES OF THE BREATHING CASE

In this section we shall discuss our numerical results and scaling properties for the breathing case of the oval billiard. Results for the scaling considering the nonbreathing geometry will be published elsewhere in the future since the range of control parameters to be studied is rather larger than for the breathing case.

The quadruple precision used in Fig. 2 causes the simulation to be extremely time consuming for the case considering ensemble averages. Since we should consider such averages to have a representative statistics for the average velocity, we now consider only double precision in our simulation. Then, solution of Eq. (6) is obtained for accuracy 10^{-13}. Thus, the average velocity obtained along the orbit is defined as

$$V_i=\frac{1}{n}\sum_{j=1}^{n}V_{i,j}, \tag{18}$$

where the index i corresponds to a sample of an ensemble of initial conditions. Finally, the average velocity is written as

$$\bar{V}=\frac{1}{M}\sum_{i=1}^{M}V_i, \tag{19}$$

where M denotes the number of particles (different initial conditions) considered. We have considered $M=500$ in our simulations. Each initial condition has a fixed initial velocity and randomly chosen $\alpha_0\in[0,\pi]$, $\theta_0\in[0,2\pi]$, and $t_0\in[0,2\pi]$.

The first step that should be addressed is the importance of the initial velocity and its influence on the behavior of $\bar{V}$. Thus, it is shown in Fig. 4 the behavior of $\bar{V}$ versus n for the control parameters $p=2$, $\epsilon=0.2$, and $\eta=0.01$ and three different initial velocities. For low initial velocity (say, $V_0=10^{-2}$, see the figure), we see that the average velocity grows and then it experiences a crossover. From there, the slope of growth is rather different from the previous region. Considering now the case of $V_0=10^{-1}$, the average velocity experiences two crossovers. At first, the average velocity is almost constant (for $n<10$). Then, it bends toward the regime of growth with the slope of the average velocity curve generated for the $V_0=10^{-2}$, reaching it around $n=10^3$ and following it. Finally, the case of $V_0=1$ shows a large plateau for the average velocity up to $n\approx10^5$. After that, it experiences a small decay and then bends toward a regime of growth with the same slope as that one marked by the two previous curves. Thus such behavior characterizes that the curves obey an envelope of growth. Note, however, that the crossover iteration number that marks the change from a constant value to a regime of growth depends on V_0. Moreover, we can see that a large initial velocity V_0 yields in a large value for the crossover.

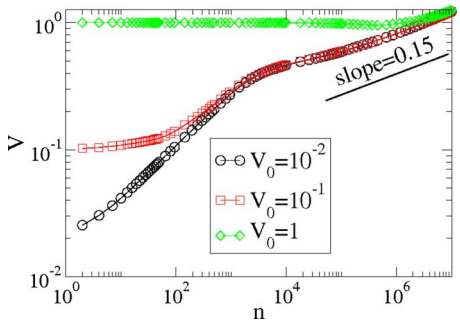

FIG. 4. (Color online) Behavior of $\bar{V}$ vs n. The control parameters used in the construction of the figure were $p=2$, $\epsilon=0.2$, $\eta=0.01$ and three different initial velocities $V_0=10^{-2}$ (circle), $V_0=10^{-1}$ (square), and $V_0=1$ (lozenge).

We now concentrate to characterize the behavior of the average velocity in terms of the number of collisions with the boundary and as a function of the control parameter η. We therefore will assume as fixed the initial velocity $V_0=10^{-3}$ and consider an ensemble of $M=500$ different initial values for $\alpha_0\in[0,\pi]$, $\theta_0\in[0,2\pi]$, and $t_0\in[0,2\pi]$. The behavior of $\bar{V}$ versus n for different values of η is shown in Fig. 5(a). We can see that all the curves start growing with a large slope, after a short transient, and then they bend toward a regime of growth with a lower exponent. The crossover number that marks the changeover from the regime of a fast

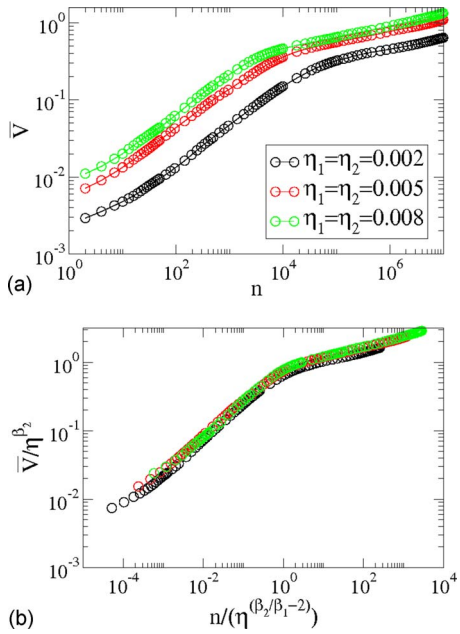

FIG. 5. (Color online) (a) Behavior of $\bar{V}$ vs n for different values of η, as labeled in the figure. The control parameters used in the construction of the figure were $p=2$, $\epsilon=0.4$ and $M=500$ different initial conditions for the same initial velocity $V_0=10^{-3}$. (b) Merger of the curves shown in (a), after an appropriate rescaling in the axis, into a single and universal curve.

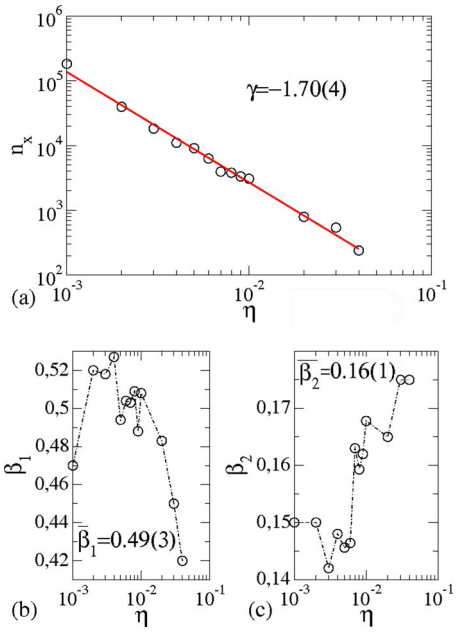

FIG. 6. (Color online) (a) Behavior of n_x vs η. A power law fitting furnishes $\gamma=-1.70(4)$. (b) The critical exponent β_1 vs η, where the average value is $\beta_1=0.49(3)$. (c) Critical exponent β_2 vs η. The average value is $\beta_2=0.16(1)$.

growth to the regime of low growth changes as the control parameter varies. Based on such kind of behavior, we can propose the following scaling hypotheses to describe the behavior of $\bar{V}$.

(1) For a small number of collisions of the particle with the boundary, i.e., $n \ll n_x$, the average velocity is described by

$$\bar{V} \propto n^{\beta_1} \quad \text{for} \quad n \ll n_x, \tag{20}$$

where β_1 is a critical exponent.

(2) Considering the case where $n \gg n_x$, the average velocity is described as

$$\bar{V} \propto n^{\beta_2} \quad \text{for} \quad n \gg n_x, \tag{21}$$

where β_2 is also a critical exponent.

(3) The crossover iteration number, i.e., the number of collisions that mark the changeover from one kind of growth to another one is given by

$$n_x \propto \eta^{\gamma}, \tag{22}$$

where the exponent γ denotes the dynamical exponent.

The critical exponents can be obtained for different curves generated for different control parameters. After some extensive simulation, we obtain that $\gamma=-1.70(4)$, $\beta_1=0.49(3)$, and $\beta_2=0.16(1)$, as they are shown in Fig. 6.

Using a similar procedure as that one used in Refs. 5 and 21 and considering the transformation $n \to n\eta^2$ to yield the description in the best scaling variables, it is easy to obtain

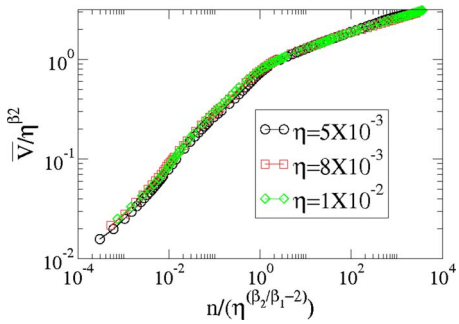

FIG. 7. (Color online) Merger of different curves of $\bar{V}$ generated by different combinations of control parameters onto a single and universal plot. The control parameters used to construct the figure were $p=3$, $\epsilon=0.3$ and the initial velocity $V_0=10^{-3}$. The parameter η is labeled in the figure.

$$\gamma = \frac{\beta_2}{\beta_1} - 2. \tag{23}$$

Evaluating Eq. (23) with both critical exponents β_1 and β_2 leads to $\gamma=-1.6735(4)$, which is quite close to the value obtained numerically.

To check whether the critical exponents and scaling hypotheses are correct, we could now try to merge all of the curves generated by the average velocity shown in Fig. 5(a) into a single and universal plot. Such merger happens after a suitable rescaling on the axis, as it is shown in Fig. 5(b).

We have also considered other combination of control parameters. The results for the case of $p=3$, $\epsilon=0.3$ and initial velocity $V_0=10^{-3}$ produced the critical exponents $\beta_1=0.48(2)$ and $\beta_2=0.15(1)$. Evaluating Eq. (23), we found that $\gamma=-1.687(8)$. It is shown in Fig. 7 the merger of three different curves generated for different control parameters. Therefore, after a suitable change in variable, both coalesce together onto a single and universal plot. This is a confirmation that the scaling properties might also be observed for other combinations of control parameters.

The obtained exponents are different from those obtained for the bouncer model (see Refs. 8 and 9 for a glance at a dissipative bouncer model and Ref. 22 for results on the Chirikov's standard map). The difference refers basically to the dimensionality of the model. Even for the breathing geometry, depending on the control parameters, the boundary of the model exhibits pieces of the boundary with nonpositive curvature, a property that is absent in the bouncer model.

IV. CONCLUDING REMARKS

As a summary of this work, we have studied the oval billiard considering the case of time perturbation of the boundary. The principal focus is the breathing geometry. We have shown that the average velocity of the particle grows to start with for small iterations with a critical exponent $\beta_1 \cong 0.5$ and then it bends toward a regime of low velocity growth with $\beta_2 \cong 0.16$. However, the regime of growth strongly depends on the initial velocity. A large value for the initial velocity yields a large value of n to produce the beginning of Fermi acceleration. The results presented in this paper do not contradict a previous paper.[20] They only reinforce that the Fermi acceleration phenomenon is quite sensi-

tive to the initial velocity, thus happening shortly for small initial velocities and longer for large values of the initial velocity. We emphasize that the dependence of the Fermi acceleration on the initial velocity has been considered in Refs. 5, 14, and 23. For the range of control parameters considered in this paper, we can conclude that the breathing geometry leads to a lower energy growth as compared to the no breathing case. We have also used scaling arguments to describe the average velocity in terms of both n and the control parameter η. Our results confirm that the velocity of the particle grows even for the breathing case, therefore reinforcing the LRA conjecture.

ACKNOWLEDGMENTS

E.D.L. thanks the support from CNPq, FUNDUNESP, and FAPESP Brazilian agencies. D.F.M.O. thanks the FAPESP and CAPES. A.L. thanks the support from FAPESP and also acknowledges the kind hospitality of DEMAC from the time of his stay in Brazil.

APPENDIX: STATIC OVAL BILLIARD

Let us shortly discuss some dynamical properties of the static oval billiard. The billiard boundary is defined as $R(\theta,p,\epsilon)=1+\epsilon\cos(p\theta)$ (see Ref. 24 for a historical review and Ref. 25 for recent results). For the case of $\epsilon=0$ the circle billiard is recovered. The two dynamical variables that describe the model are α_n and θ_n, where α denotes the angle of the trajectory measured with respect to the tangent vector at the angular position θ. The mapping that describes such a model is given by

$$R(\theta_{n+1})\sin(\theta_{n+1}) - Y(\theta_n) = \tan(\alpha_n+\phi_n)[R(\theta_{n+1})\cos(\theta_{n+1}) - X(\theta_n)], \tag{A1}$$

$$\alpha_{n+1} = \phi_{n+1} - (\alpha_n+\phi_n), \tag{A2}$$

where $X(\theta_n)=R(\theta_n)\cos(\theta_n)$, $Y(\theta_n)=R(\theta_n)\sin(\theta_n)$, and $\phi_n=\text{atan}[Y'(\theta_n)/X'(\theta_n)]$ with $X'(\theta_n)=dX(\theta_n)/d\theta_n$ and $Y'(\theta_n)=dY(\theta_n)/d\theta_n$. The phase space generated by iteration of Eqs. (A1) and (A2) is shown in Figs. 8(a) and 8(b). The control parameters used were $p=2$ and (a) $\epsilon=0.1$ and (b) $\epsilon=0.21$. We can see in Fig. 8(a) the mixed structure including KAM islands, a chaotic sea, and invariant spanning curves. However, for a control parameter larger then the critical value $\epsilon_c=1/(1+p^2)$, all the invariant spanning curves are destroyed, as can be seen in Fig. 8(b). Such a destruction is due to the boundary that now exhibits some regions of negative curvature. The numbered regions shown in Fig. 8(a) corresponding to periodic and quasiperiodic behavior are illustrated in Fig. 9. Region 1 corresponds to librational motion, as shown in Fig. 9(a), while region 2 corresponds to a rotational motion, as illustrated in Fig. 9(b). Such orbits indeed travel very near the boundary. Finally region 3 identifies the motion as rotational, as shown in Fig. 9(c).

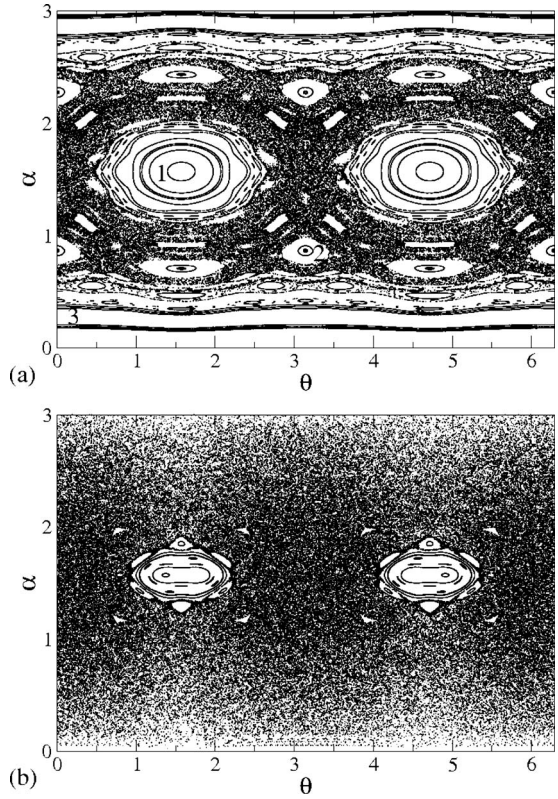

FIG. 8. Phase space for the static oval billiard. The control parameters used in the construction of the figure were $p=2$ and (a) $\epsilon=0.1$ and (b) $\epsilon=0.21$.

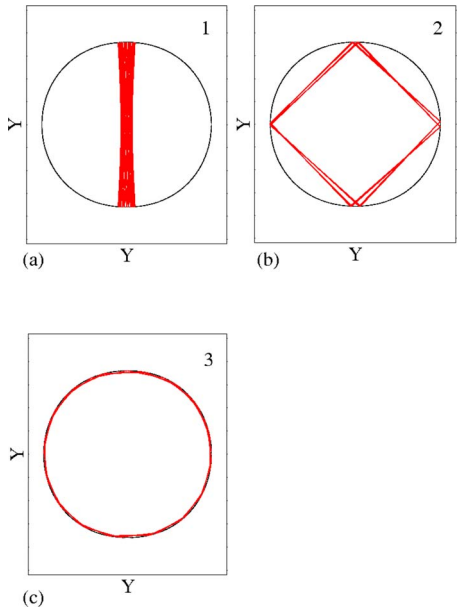

FIG. 9. (Color online) Typical orbits in the oval billiard. (a) Librational motion. (b) Rotational motion around a period four. (c) Rotational motion around an invariant spanning curve.

[1]E. Fermi, Phys. Rev. **75**, 1169 (1949).
[2]A. J. Lichtenberg and M. A. Lieberman, *Regular and Chaotic Dynamics*, Applied Mathematical Sciences Vol. 38 (Springer-Verlag, Berlin, 1992).
[3]L. D. Pustilnikov, Trudy Moskow Mat. Obshch. **34**, 1 (1977).
[4]A. K. Karlis, P. K. Papachristou, F. K. Diakonos, V. Constantoudis, and P. Schmelcher, Phys. Rev. Lett. **97**, 194102 (2006); Phys. Rev. E **76**, 016214 (2007).
[5]E. D. Leonel, P. V. E. McClintock, and J. K. L. da Silva, Phys. Rev. Lett. **93**, 014101 (2004).
[6]R. M. Everson, Physica D **19**, 355 (1986).

[7]P. J. Holmes, J. Sound Vib. **84**, 173 (1982).
[8]E. D. Leonel and A. L. P. Livorati, Physica A **387**, 1155 (2008).
[9]A. L. P. Livorati, D. G. Ladeira, and E. D. Leonel, Phys. Rev. E **78**, 056205 (2008).
[10]J. J. Barroso, M. V. Carneiro, and E. E. N. Macau, Phys. Rev. E **79**, 026206 (2009).
[11]E. D. Leonel and P. V. E. McClintock, J. Phys. A **38**, 823 (2005).
[12]D. G. Ladeira and E. D. Leonel, Chaos **17**, 013119 (2007).
[13]D. F. M. Oliveira, R. A. Bizão, and E. D. Leonel, "Scaling properties of a hybrid Fermi-Ulam-Bouncer model," Math. Probl. Eng. (in press).
[14]A. Loskutov, A. B. Ryabov, and L. G. Akinshin, J. Phys. A **33**, 7973 (2000).
[15]S. O. Kamphorst and S. P. de Carvalho, Nonlinearity **12**, 1363 (1999).
[16]R. E. de Carvalho, F. Caetano de Souza, and E. D. Leonel, J. Phys. A **39**, 3561 (2006).
[17]J. Koiller, R. Markarian, S. O. Kamphorst, and S. P. de Carvalho, J. Stat. Phys. **83**, 127 (1996).
[18]F. Lenz, F. K. Diakonos, and P. Schmelcher, Phys. Rev. Lett. **100**, 014103 (2008).
[19]V. Gelfreich and D. Turaev, J. Phys. A: Math. Theor. **41**, 212003 (2008).
[20]S. O. Kamphorst, E. D. Leonel, and J. K. L. da Silva, J. Phys. A: Math. Theor. **40**, F887 (2007).
[21]E. D. Leonel, Phys. Rev. Lett. **98**, 114102 (2007).
[22]D. G. Ladeira and J. K. L. da Silva, J. Phys. A: Math. Theor. **40**, 11467 (2007).
[23]A. Loskutov and A. B. Ryabov, J. Stat. Phys. **108**, 995 (2002).
[24]M. V. Berry, Eur. J. Phys. **2**, 91 (1981).
[25]D. F. M. Oliveira and E. D. Leonel, "On the dynamical properties of an elliptical/oval billiard with static boundary," Commun. Nonlinear Sci. Numer. Simul. (in press).